Strategic timing of contralateral nephrectomy after ischemic acute kidney injury prevents chronic kidney disease by enhancing progenitor proliferation, attenuating polyploidization and reshaping the immune response

see commentary on page 533

OPEN

Lies Moonen[1,9], Carolina Conte[2,9], Elien Van Campen[1,3,9], Anna Julie Peired[4], Letizia De Chiara[2], Pourya Pilva[3], Bart Cuypers[5], Pieter Meysman[5], Fabio Affaticati[5], Kris Laukens[5], Cristina Cuesta-Apausa[6], Stuart Maudsley[7], Tom Vanden Berghe[1], Patrick C. D'Haese[1], Paola Romagnani[2,4], Peter Boor[3,8], Elena Lazzeri[2,10] and Benjamin A. Vervaet[1,3,10]

[1]Cell Death Signaling Lab, Department of Biomedical Sciences, Inflamed Centre of Excellence, University of Antwerp, Antwerp, Belgium; [2]Department of Experimental and Clinical Biomedical Sciences "Mario Serio", University of Firenze, Florence, Italy; [3]Institute of Pathology, RWTH Aachen University Hospital, Aachen, Germany; [4]Nephrology and Dialysis Unit, Meyer Children's Hospital, IRCCS, Florence, Italy; [5]Adrem Data Lab, Department of Computer Science, University of Antwerp, Antwerp, Belgium; [6]Centro de Investigación del Cáncer, Consejo Superior de Investigaciones Científicas (CSIC), University of Salamanca, Salamanca, Spain; [7]Receptor Biology Lab, Department of Drug Discovery, Moffit Cancer Center, Tampa, Florida, USA; and [8]Electron Microscopy Facility, RWTH Aachen University Hospital, Aachen, Germany

Abstract

Introduction: Kidneys have a limited capacity for self-repair, and injury frequently progresses to chronic kidney disease (CKD). Remarkably, successful recovery is observed in models of unilateral acute kidney injury (AKI) upon contralateral nephrectomy. Here, we aim to better understand the cellular and molecular mechanisms underlying this enhanced recovery.

Methods: Six rodent studies were performed, including optimization and time-course experiments in Wistar rats and C57BL/6J mice to define left ischemia conditions, right nephrectomy delay times, and functional outcome. Kidneys were analyzed by quantitative histomorphometry (pathomics) on whole slide sections, immunostaining, and qPCR. Bulk RNA sequencing was conducted in two independent mouse time-course studies to discern repair and injury trajectories. Clonal expansion of tubular progenitor cells was assessed by lineage tracing in PAX2/Confetti mice. Tubular epithelial cell proliferative dynamics and polyploidization were analyzed using live cell cycle and DNA content profiling in PAX8/FUCCI2aR mice.

Results: Nephrectomy at day three after AKI induced full functional recovery in rats and mice, whereas longer delays (10 and 20 days) failed to prevent CKD progression. Early nephrectomy reduced tubular atrophy, fibrosis, and inflammation. Pathomics revealed distinct tubular morphological trajectories distinguishing between atrophy and repair, as adaptive signatures. Transcriptomic analyses with orthogonal validation demonstrated attenuation and reshaping of immune cell signatures and inflammatory pathways. Additionally, specific gene sets unique to nephrectomy-induced repair were identified. Lineage tracing showed that nephrectomy enhanced clonal expansion of tubular progenitor cells, beyond the levels of spontaneous repair. Cell cycle and DNA-content analysis of tubular cells demonstrated a strong polyploid response immediately after the ischemic insult, while early nephrectomy attenuated persistent tubular cell polyploidization, a contributor to CKD.

Conclusions: Early nephrectomy in experimental AKI triggers efficient repair by modulating immune responses, promoting tubular regeneration, inducing pro-repair transcriptional reprogramming, and counteracting progression to CKD through attenuation of sustained polyploidization.

Kidney International (2026) **110,** 664–680; https://doi.org/10.1016/j.kint.2026.04.035

KEYWORDS: immune modulation; kidney repair; nephrectomy; polyploidy; progenitor cells; regeneration

© 2026 THE AUTHORS. Published by Elsevier Inc. on behalf of the International Society of Nephrology. This is an open access article under the CC BY-NC license (http://creativecommons.org/licenses/by-nc/4.0/).

Correspondence: *Benjamin A. Vervaet, Institute of Pathology, RWTH Aachen University Hospital, Pauwelsstrasse 30, 52074 Aachen, Germany or Cell Death Signaling Lab, University of Antwerp, Universiteitsplein 1, 2610 Antwerp, Belgium. E-mail: bvervaet@ukaachen.de and benjamin.vervaet@uantwerpen.be*

[9]LM, CC, and EVC equally contributed.

[10]EL and BAV equally contributed.

Received 6 January 2025; revised 31 March 2026; accepted 6 April 2026; published online 15 June 2026

The incidence of acute kidney injury (AKI) has been growing since 2001 and is responsible for an in-hospital mortality rate of 40% to 50% and even >50% for intensive care unit patients in the United States.[1]

Translational Statement

Acute kidney injury (AKI) is common and frequently progresses to chronic kidney disease (CKD), with limited treatment options. Defining mechanisms that counteract the AKI-to-CKD transition may inform future therapeutic strategies. In a unilateral AKI-to-CKD model, contralateral nephrectomy performed 3 days after injury enhances intrinsic repair capacity and establishes a critical temporal window during which CKD progression can be fully prevented. Uninephrectomy induces a coordinated regenerative response exceeding spontaneous repair, characterized by immune modulation, transcriptional reprogramming, expansion of tubular progenitor cells, and mitigation of maladaptive polyploidization. This model provides a framework to dissect kidney repair plasticity and identify targets for regenerative intervention.

Clinical studies identified AKI, depending on the severity and number of insults, as an important risk factor for the development of chronic kidney disease (CKD) and renal cell carcinomas,[2,3] thereby indicating that recovery from AKI is likely not complete.[4,5]

An important cellular determinant of AKI outcomes is the behavior of the tubular epithelial cells (TECs) that survive the primary insult. Two main spontaneous response mechanisms have been identified.[6] First, TECs regenerate by proliferation to replace their lost neighbors. Although there is no consensus on the main driving cell population, both mature cells and progenitor cells were suggested to be involved in tubular repair.[7,8] Second, a major portion of remnant mature TECs undergo polyploidization-mediated hypertrophy.[6,9] In this process, cells become polyploid to increase their working capacity to rapidly ensure life-saving compensation for the acute loss of organ function while regenerative proliferation initiates in the background.[9,10] However, polyploid TECs are also known to drive adverse long-term sequelae after AKI because of their excessive and persistent secretion of profibrotic factors, as described in other organs.[9–19]

To date, there are no adequate therapies that directly target the injured kidney. The current understanding of cellular mechanisms of kidney recovery after AKI is mainly based on studying the course of animal models after ischemic, toxic, or obstructive injury. However, there is an intriguing phenomenon where functional and histologic recovery of a single injured kidney is naturally enhanced by the removal of the contralateral unharmed kidney.[20–22] When the contralateral kidney is left in place, the acutely injured kidney progresses to atrophy and fibrosis (i.e., undergoing the AKI-to-CKD transition).[22–24] This rescuing phenomenon, first reported by Hinman in the early 1920s, is known as nephrectomy (Nx)–induced recovery.[20–22]

Although preservation or increase of mass has been reported in injured kidneys after contralateral Nx,[25–27] the fundamental question of whether Nx stimulates tubular epithelial regeneration is left unanswered. In addition, it is known that Nx can attenuate inflammation[28,29]; however, its impact on the inflammatory landscape is still only partially understood. In the present study, we explored this phenomenon and (i) optimized rat and murine models of Nx-induced recovery that lead to full or partial functional restoration, (ii) defined structural, fibrotic, and inflammatory outcomes, (iii) quantified whether and to what extent Nx-induced recovery is associated with proliferation of tubular progenitor cells, (iv) evaluated whether Nx affects polyploidization-mediated hypertrophy of TECs, and (v) identified a robust prorepair gene signature.

METHODS

Animals and experimental design

Six different animal experiments were set up, including a 63-day time course study in Wister rats with varying right Nx delay times (days 3, 10, and 20) after left unilateral ischemia-reperfusion injury (UIRI; 60-minute ischemia at 35 °C), a 7-day UIRI-Nx model optimization study in C57BL/6J mice (21-, 23-, or 30-minute ischemia at 34 °C, 35 °C, 36 °C, or 37 °C), a 7- and 42-day UIRI-Nx time course study in C57BL/6J mice (21-minute ischemia at 36 °C and 34 °C, respectively), a 30-day lineage tracing study of epithelial progenitor cells in the UIRI-Nx model in PAX2/Confetti mice (21-minute ischemia at 36 °C), and, finally, a 30-day cell cycle/DNA content study of TECs in the UIRI-Nx model in PAX8/FUCCI2aR mice (21-minute ischemia at 36 °C) (Supplementary Methods and Supplementary Figure S1). All animal procedures were conducted according to the National Institute *Guide for the Care and Use of Laboratory Animals* and approved by the University of Antwerp Ethics Committee (approval numbers 2017-36, 2011-51, 2016-15, and 2024-34) or the Institutional Animal Care and Use Committee of the University of Florence, Italy, and by the Italian Ministry of Health (approval numbers 264/2020-PR and 864/2021-PR).

Histology

Kidney morphology was assessed using periodic acid–Schiff staining. Sirius red staining was used to analyze fibrosis. Antibodies for staining kidney damage and inflammation are provided in the Supplementary Methods.

Real-time quantitative polymerase chain reaction

Total mRNA was extracted from the ischemic kidney (PureLink RNA Mini Kit; Life Technologies Belgium) and converted to cDNA (High-Capacity cDNA archive kit; Life Technologies Belgium). Real-time polymerase chain reaction (PCR) amplification was performed using QuantStudio 3 Real-Time PCR System (Applied Biosystems) and ABI Prism 7300 sequence detector (Applied Biosystems). TaqMan probes and primer sequences are given in the Supplementary Methods and Supplementary Table S1.

Pathomics

Quantitative histomorphometric analysis was performed on whole-slide images of periodic acid–Schiff–stained kidney sections from the C57BL6/J time course study (n = 48) by a computational method for high-throughput morphologic feature extraction, as previously described.[30]

Transcriptomics

Bulk RNA sequencing was performed on total mRNA extracted from kidney samples from 2 independent C57BL/6J time-course studies (21-minute ischemia at 34 °C–36 °C) (Supplementary Methods and Supplementary Table S2). The analyzed groups included control, UIRI day 3, UIRI day 7, and UIRI + Nx day 7. To isolate the effect of Nx, data analysis focused on 4 complementary comparisons: first, UIRI + Nx day 7 with UIRI day 7 to capture the overall difference at day 7 (the day 7 comparison); second, time-course changes from UIRI day 3 to UIRI + Nx day 7 (the repair trajectory) and UIRI day 3 to UIRI day 7 (the injury trajectory); third, identification of differentially expressed genes (DEGs) in the repair trajectory (UIRI day 3 to UIRI + Nx day 7) excluding DEGs shared with the injury trajectory (UIRI day 3 to UIRI day 7) to isolate genes unique to the repair trajectory; and fourth, identification of counter-regulated genes between the 2 trajectories (Supplementary Methods and Supplementary Table S3).

Proliferation of PAX2$^+$ tubular progenitors and polyploidization of TECs

Proliferation of PAX2$^+$ tubular progenitors was analysed using lineage tracing and clone size frequency analysis in PAX2-Confetti mice, as described earlier.[7] Polyploidization of TECs was analyzed through live cell cycle and DNA content analyses in PAX8-FUCCI2aR mice.

Statistics

Statistical analyses were performed using Prism GraphPad (version 9.5.0.730), OriginPro (Research Resource Identifier [RRID]: SCR015636) and OriginPro2026 (OriginLab Corporation), and R Studio (v 4.2.2).

Further method details are provided in the Supplementary Methods.

RESULTS

Timing of contralateral Nx after AKI determines recovery

In rats, Nx performed 3 days after UIRI induced full functional recovery of the injured kidney from day 35 after Nx onward. Nx performed on day 10 or 20 after UIRI led to only partial recovery, with glomerular filtration rate remaining approximately 30% lower than controls by the study end point ($P < 0.05$) (Figure 1a and b). Although kidney function after Nx on day 10 was not significantly different from that observed after Nx on day 3, only the latter normalized kidney function to control levels (Figure 1b). When Nx was delayed until 24 hours before the study end point, remnant kidney function decreased by 56% (Figure 1b). Kidney collagen content, assessed by Sirius red staining, remained at control levels when Nx was performed on day 3 after UIRI. Longer Nx-delay times did not attenuate collagen deposition (Figure 1c and d). Interestingly, Nx consistently suppressed CD45$^+$ leukocyte infiltration regardless of Nx delay time (Supplementary Results and Supplementary Figure S2). Collectively, these data demonstrate that if Nx is performed early after AKI, it can induce a complete recovery of kidney function, whereas later Nx is less effective.

Nx ameliorates kidney injury

First, we established the model of full recovery (i.e., with Nx 3 days after UIRI) in C57BL/6J mice (Supplementary Results and Supplementary Table S4). As in rats, UIRI alone led to a progressive decline of kidney function (8-fold increase in serum creatinine, $P < 0.01$), which was completely rescued by Nx by day 42 (Figure 2a). Kidney injury molecule-1 immunostaining as tubular injury marker was elevated at day 3 after UIRI compared with controls (16.5% ± 3.1% vs. 0.2% ± 0.1%; $P < 0.001$) and remained increased until day 21 (Figure 2b and c). In comparison to the UIRI group, the UIRI + Nx group exhibited similar levels of kidney injury molecule-1 at day 7 but significantly lower levels at day 21 (1.1% ± 0.4% vs. 3.7% ± 1.9%; $P < 0.05$). Reduction of *Kim-1* mRNA expression approaching normal levels was noted in the UIRI + Nx group (Figure 2d). Similar results were found for a second tubular injury marker (i.e., *Lcn2* or neutrophil gelatinase–associated lipocalin) (Figure 2e).

Nx prevents kidney atrophy and fibrosis

Macroscopically, UIRI induced a progressive loss of mass of the injured kidney by 35% and 50% at 21 and 42 days after UIRI in C57BL/6J mice, respectively (Figure 3a and b). Contralateral Nx prevented the loss of kidney mass (Figure 3a and b), and from day 4 after Nx, a significant increase in kidney weight was observed compared with controls. The weight of the contralateral kidney in UIRI did not change significantly compared with control kidneys throughout the follow-up (Figure 3b).

Qualitative microscopic histopathologic assessment on periodic acid–Schiff staining showed that UIRI without Nx led to tubular atrophy and interstitial fibrosis, which both were prevented by Nx (Figure 3c). Pathomics revealed a progressive reduction of tubular area after UIRI from day 3 onwards, resulting in a 22% loss on day 42 compared with controls (Figure 3d). In the UIRI group, the tubular diameters (μm) and area percentage shrank to 84.7% and 68.2% of control values from day 3 onwards, respectively, reflecting tubular atrophy (Figure 3d–f, Supplementary Results, and Supplementary Figure S3A–L). Tubular density (i.e., the number of tubules per mm^2) showed a transient increase, peaking at day 3 after UIRI and normalizing to control levels by day 42, mainly in the cortex (Figure 3g). Nx prevented these alterations, with only 5.5% loss of tubular area compared with controls, preservation of the average tubular diameter and areas, and normalization of tubular density (Figure 3d–g). The tubular diameters and size

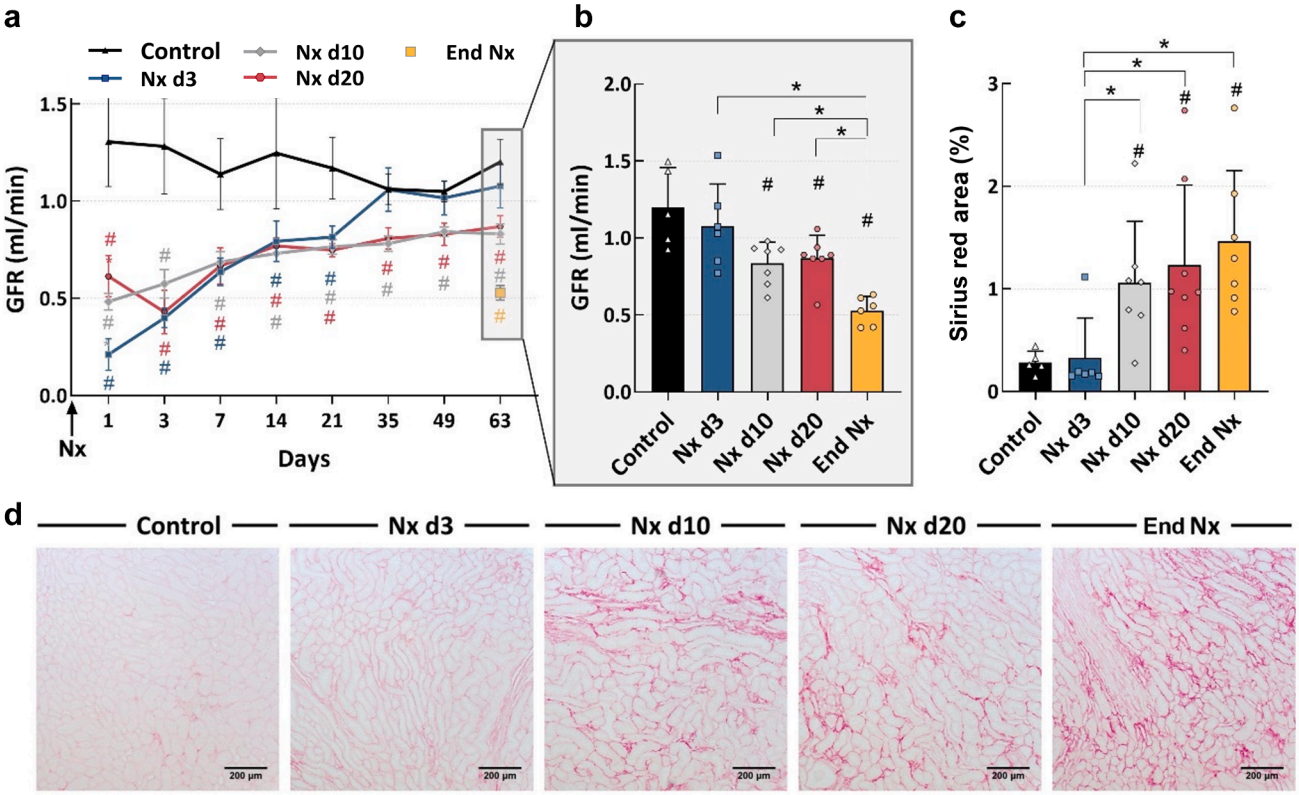


Figure 1 | Determination of transcutaneous glomerular filtration rate (GFR) in rats. (**a**) Transcutaneous GFR at intermediate time points after (sham-)nephrectomy (Nx) in controls (n = 5) and animals with Nx on day (d) 3 (n = 6), day 10 (n = 7), day 20 (n = 8), or end Nx (n = 6). (**b**) End-point transcutaneous GFR on day 63. GFR was measured 24 hours after removal of the contralateral kidney on day 62, to ensure that measurements only rely on the injured kidney's function. (**c**) Histologic quantification of Sirius red staining on day 63 in controls (n = 5) and animals with Nx on day 3 (n = 6), day 10 (n = 7), day 20 (n = 8), or end Nx (n = 7). (**d**) Representative images of Sirius red staining on day 63. Bar = 200 µm. Data are presented as mean ± SEM (**a**) and mean + SD (**b,c**). *$P < 0.05$ between groups, #$P < 0.05$ versus control. To optimize viewing of this image, please see the online version of this article at www.kidney-international.org.

distributions shifted from a bimodal pattern in controls, reflecting distinct average cortical and medullary tubular diameters, to a more equalized distribution (Figure 3f, Supplementary Results, and Supplementary Figure S3A–C and G–I).

Pathomics further demonstrated a steady increase in interstitial area (surrogate for interstitial fibrosis) after UIRI, reaching its maximum by day 21 (Figure 3h and i). Nx prevented this progression but with an interstitial area remaining approximately 6.5% higher compared with controls from day 7 onwards (Figure 3h). The density ridgeline plot of the interstitial area illustrated the distinct kidney trajectories between UIRI with and without contralateral Nx (Figure 3i).

Analysis of the fibrotic response by Sirius red staining in UIRI mice confirmed the progressive increase of tubulointerstitial collagen deposition in the injured kidney (Figure 3j and k). Nx attenuated tubulointerstitial fibrosis, with levels comparable to controls by day 42 (Figure 3j and k). Gene expression analysis of the profibrotic cytokine *Tgfβ* revealed a persistent upregulation from day 3 after UIRI onwards (4-fold), with a 9-fold increase at day 21 compared with controls (Figure 3l). In the UIRI + Nx group, *Tgfβ* expression in the injured kidney was consistently lower compared with the UIRI group from day 7 onwards and even reached control levels by day 42.

Nx attenuates and reshapes the immune response

To capture the early overall state difference at day 7, bulk RNA-sequencing comparison of UIRI day 7 to UIRI + Nx day 7 identified 2406 significant DEGs (1090 upregulated and 1316 downregulated) in response to Nx (Supplementary Results, Supplementary Figure S4, Supplementary Table S5, and Supplementary Data S1). To identify Nx-affected functional processes, Gene Ontology enrichment analysis was performed on these DEGs. In total, 2004 DEGs were mapped to 375 pathways (at $P < 0.05$ significance level), of which 119 were positively and 256 were negatively enriched (Figure 4a and b). The upregulated genes are strongly enriched for organic, oxoacid, carboxylic acid, small-molecule, and lipid metabolism, indicating metabolic reprogramming typically characteristic of increased mitochondrial activity, enhanced energy metabolism, and shifts in substrate use (amino acids, fatty acids, and organic acids) (Figure 4a). The

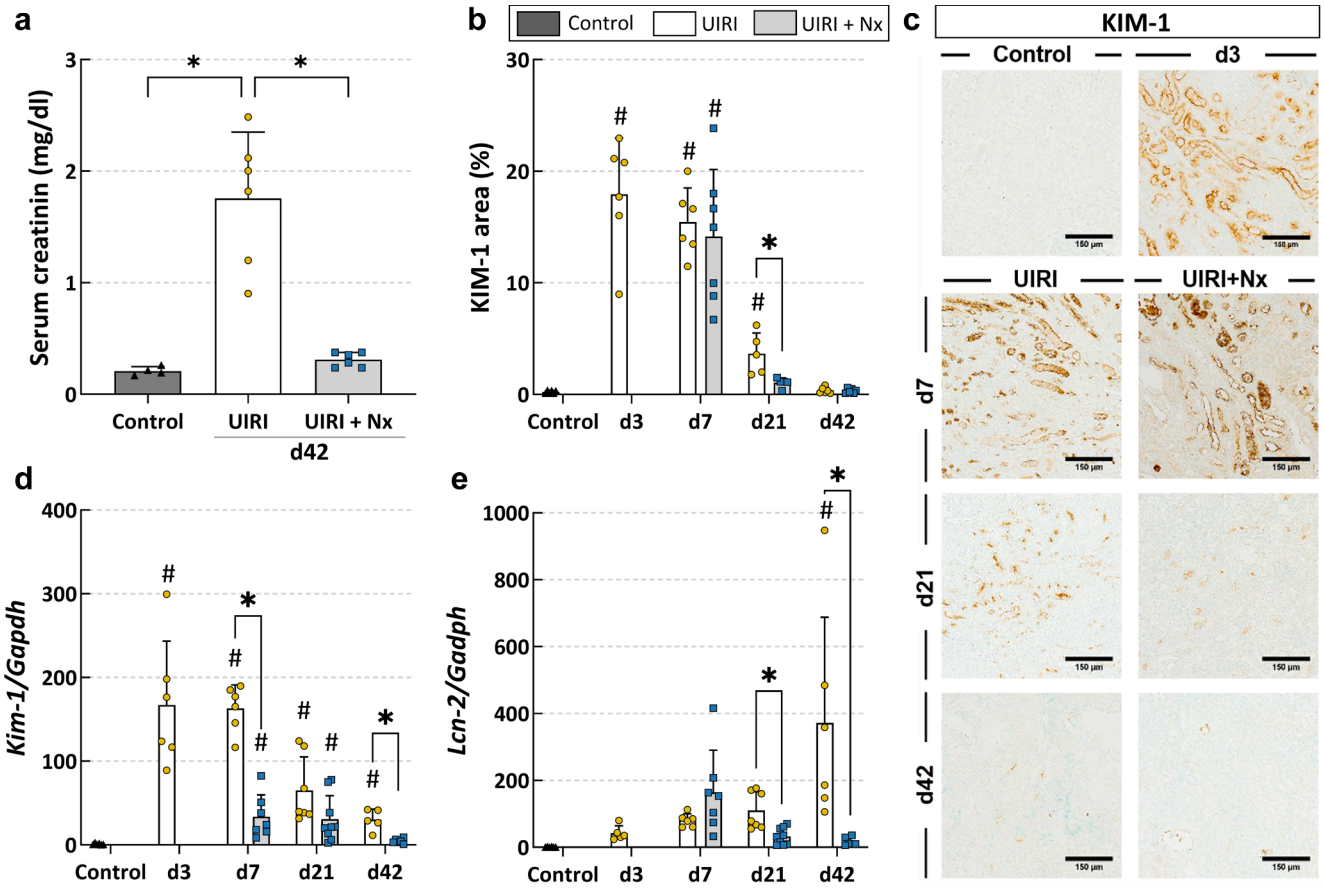


Figure 2 | Evaluation of kidney function and injury parameters. (**a**) Serum creatinine measured on day 42, in control animals (n = 4), unilateral ischemia-reperfusion injury (UIRI) animals (n = 6), and UIRI + nephrectomy (Nx) animals (n = 6). In the UIRI day (d) 42 group, kidney function was measured 24 hours after removal of the contralateral kidney at day 41 to ensure that measurements only rely on the injured kidney's function. (**b**) Histologic quantification of kidney injury molecule 1 (KIM-1) staining in control animals (n = 6) and animals euthanized 3 days (n = 6), 7 days (UIRI n = 6; UIRI + Nx n = 7), 21 days (UIRI n = 5; UIRI + Nx n = 5), or 42 days (UIRI n = 6; UIRI + Nx n = 6) after UIRI. (**c**) Representative images of KIM-1 staining. Bar = 150 μm. (**d**) Kim-1 gene expression by quantitative polymerase chain reaction (qPCR) in control animals (n = 6) and animals euthanized 3 days (n = 6), 7 days (UIRI n = 6; UIRI + Nx n = 7), 21 days (UIRI n = 7; UIRI + Nx n = 9), or 42 days (UIRI n = 5; UIRI + Nx n = 6) after UIRI. (**e**) *Lcn2* gene expression by qPCR control animals (n = 6) and animals euthanized 3 days (n = 5), 7 days (UIRI n = 6; UIRI + Nx n = 7), 21 days (UIRI n = 7; UIRI + Nx n = 9), or 42 days (UIRI n = 6; UIRI + Nx n = 6) after UIRI. In all UIRI + Nx groups, Nx was performed 3 days after UIRI. Data are presented as mean + SD. *$P < 0.05$ between groups; #$P < 0.05$ versus control. To optimize viewing of this image, please see the online version of this article at www.kidney-international.org.

downregulated genes revealed a clear effect on inflammatory processes, including "leukocyte activation," "lymphocyte differentiation," and "regulation of immune responses" (Figure 4b).

To evaluate the impact of Nx on immune cell composition during the early phase, we quantified relative abundance estimated for various immune cell subsets by applying single-sample gene set enrichment analysis to the bulk RNA-sequencing data.[31] Using curated gene signatures of 40 immune cell types,[32–34] we found that UIRI induced broad increases in nearly all subsets of dendritic cells, macrophages, $CD4^+$ T cells (including T helper [Th] 1 and Th17), and $CD8^+$ T cells, whereas naive $CD4^+$ (CD4_Tn) and $CD8^+$ (CD8_Tn) abundances decreased (Figure 4c–n, Supplementary Results, and Supplementary Figure S6). Nx attenuated these changes, keeping most immune cell abundances close to (or even below) their levels at day 3 after UIRI, but still higher than controls (Figure 4, Supplementary Results, and Supplementary Figure S6). Several populations remained elevated, including infiltrating macrophages (Infiltrate_Mac) and a rare M14 macrophage subset predicted from single-cell RNA sequencing to have prorepair features (Supplementary Results and Supplementary Figure S6C′).[32]

Pan-leukocyte CD45 staining confirmed the immune cell infiltration at day 7 after UIRI, its persistence up to day 42 (Figure 5a and b), and the reduction by Nx. Immunofluorescent staining for $CD68^+$ cells (monocytes), $F4/80^+$ cells (macrophages), $CD3^+$ T cells, $CD4^+$ T cells, and $CD8^+$ T cells showed substantial increases after UIRI and pronounced attenuation after Nx (Figure 5c–k, Supplementary Results, and Supplementary Figure S7), corroborating the single-sample gene set enrichment analysis predications. Likewise, mRNA expression of the proinflammatory gene *Tnfα* was

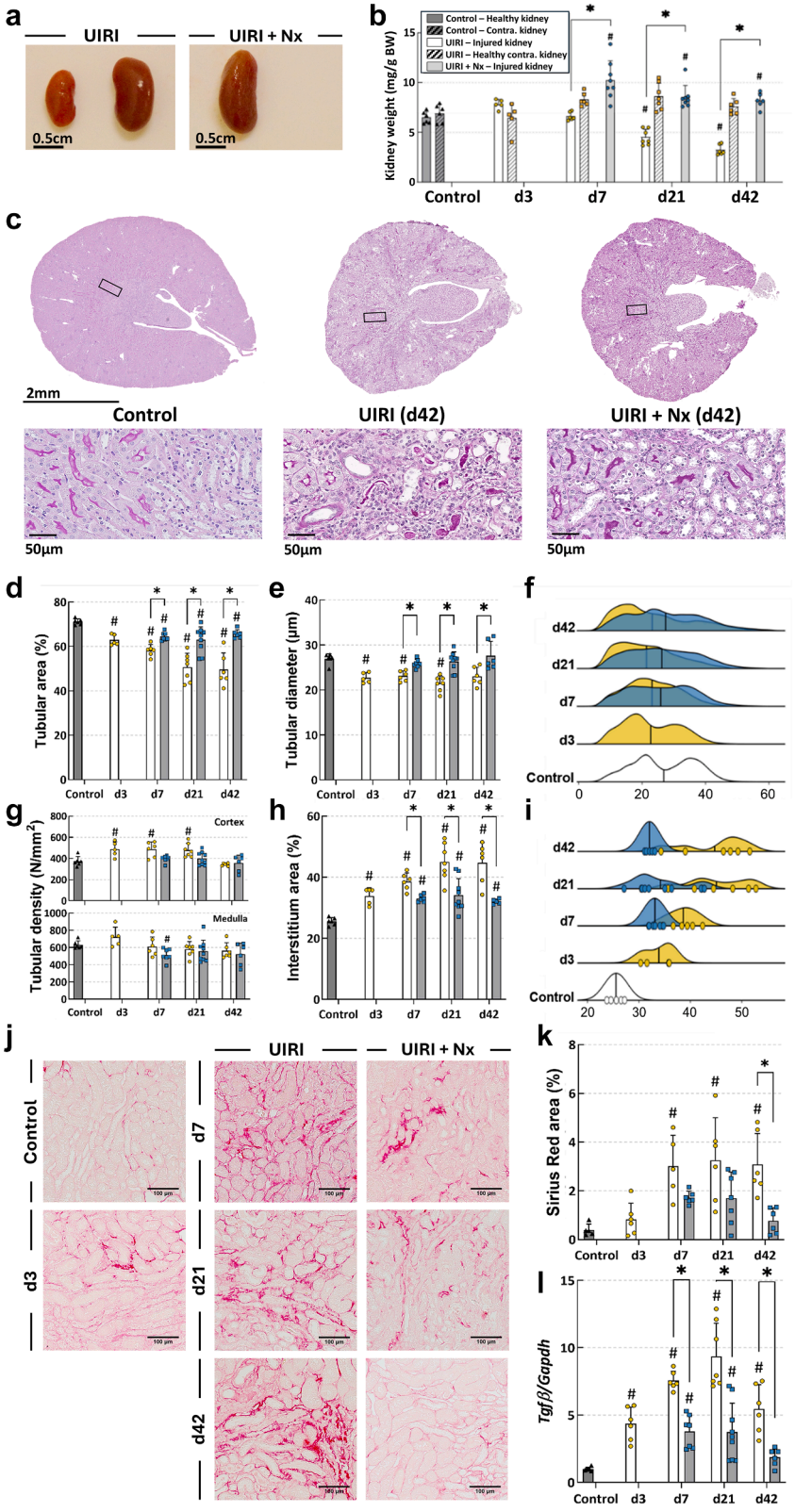


Figure 3 | Evaluation of atrophic and fibrotic response after unilateral ischemia-reperfusion injury (UIRI) with and without contralateral nephrectomy (Nx) performed on day (d) 3. (**a**) Representative macroscopic images of kidneys on day 42. (**b**) Mass of the ischemic and healthy contralateral kidneys corrected for body weight (BW) in control animals (n = 6) and animals euthanized 3 days (n = 5), 7 days (UIRI n = 6; UIRI + Nx n = 8), 21 days (UIRI n = 7; UIRI + Nx n = 8), or 42 days (UIRI n = 6; UIRI + Nx n = 6) after UIRI. (**c**) Representative cross-sections of periodic acid–Schiff staining of kidneys on day 42. (**d**) Mean tubular area per total tissue size (%) in control animals (n = 6) and animals euthanized 3 days (n = 5), 7 days (UIRI n = 6; UIRI + Nx n = 7), 21 days (UIRI n = 7; UIRI + Nx n = 9), or 42 days (continued)

persistently upregulated by UIRI (Figure 5l), whereas Nx attenuated this response. Next, because the transcriptomic analyses suggested qualitative shifts in the macrophage compartment, we performed quantitative PCR for canonical polarization markers distinguishing inflammatory (*Cd86* and *Il6*) and repair-associated (*Cd206* [*Mrc1*] and *Il10*) phenotypes (Figure 5m–p). Nx consistently suppressed *Cd86* across all time points, whereas *Il6*, *Cd206*, and *Il10* were reduced only later, indicating an early shift away from a proinflammatory macrophage profile (Figure 5m–p). The *Cd206* mRNA fraction (*Cd206*/[*Cd206* + *Cd86*]) further revealed an early shift toward prorepair macrophage phenotypes (Figure 5q).

Transcriptomics reveals a repair-associated signature after Nx

To examine the Nx-specific temporal effects, DEGs were identified per trajectory (UIRI day 3 to UIRI day 7, injury trajectory; and UIRI day 3 to UIRI + Nx day 7, repair trajectory). We found 2377 signficant DEGs (1219 upregulated and 1158 downregulated) for the injury trajectory and 2288 DEGs (1025 upregulated and 1263 downregulated) for the Nx-induced repair trajectory (Supplementary Results, Supplementary Figure S4, Supplementary Table S5, and Supplementary Data S1). Among these, 1528 significant DEGs (898 upregulated and 630 downregulated) were unique to injury, whereas 1439 significant DEGs (714 upregulated and 725 downregulated) were unique to repair (Figure 6a–d, Supplementary Results, Supplementary Table S5, and Supplementary Data S1). Of all significant DEGs, 849 (36%) were in common between the trajectories, 76 of which were contraregulated (Figure 6e). Variance-stabilized expression patterns showed clear condition-specific profiles, with UIRI + Nx day 7 samples diverging from both UIRI day 3 and UIRI day 7 (Figure 6a).

Functional annotation of genes uniquely upregulated along the repair trajectory revealed activation of specific programs, including cellular protection from damage by toxins and reactive oxygen species (glutathione S-transferase superfamily), adaptive Na^+, Ca^{2+}, and K^+ ion transport, catecholamine metabolism, and gluconeogenesis/lipid metabolism (including peroxisome proliferator–activated receptor-α–mediated fatty acid oxidation/ketogenesis) (Figure 6c, Supplementary Results, and Supplementary Table S6). Gene Ontology analysis of downregulated genes unique to the repair trajectory reveals suppression of injury-associated programs, including cell-cell adhesion (Claudin gene family), interferon/antiviral responses, organic anion transport (solute carrier [SLC] 22 family), and multiple receptor–tyrosine kinase–mediated pathways involved in vascular, stromal, and growth factor signaling (Figure 6d, Supplementary Results, and Supplementary Table S6).

We next identified the most high-confidence Nx-responsive genes by combining visual outlier detection from volcano plots with a quantitative ranking score ($-\log_{10}$ adjusted $P \times |\log_2$ fold change|) in the repair trajectory, focusing on genes with $|\log_2$ fold change$| > 1.5$ and adjusted $P < 0.05$. This approach highlighted a set of 8 upregulated (*Calb1*, *Slc38a3*, *Gsta5*, *Lpo*, *Vsig4*, *Gm12326*, *Cyp27b1*, and *Mtarc1*) and 7 downregulated genes (*Dnase1*, *Cyp2d12*, *Itih1*, *Sec14l3*, *Prss35*, and *A930038B10Rik*), reflecting a core signature of Nx-induced repair (Figure 6b). Importantly, analysis of the 2 independent bulk RNA-sequencing experiments as biological replicates yielded a consistent DEG list identifying *Calb1*, *Cyp27b1*, *Slc38a3*, *Gsta5*, *Dnase1*, *Itih1*, and *Sec14l3* among the highest-ranked genes, supporting robustness of our findings (Supplementary Results and Supplementary Table S7).

Finally, the contraregulated genes revealed a subset that distinguishes successful repair from ongoing injury, where Nx promotes metabolic reactivation (*Aass* and *Prodh*),[35,36] epithelial transport recovery (*Slc6a19* and *Mfsd4b1*),[37,38] cellular remodeling (*Ppp1r16b* and *Cwh43*),[39,40] and pro-resolving immune/vascular remodeling (*Lyve-1*),[41] while suppressing a coordinated network of interferon/Th1-driven inflammation (*Cxcl10*, *Tbx21*, and *Spib*),[42–44] cytotoxic activity (*Nkg7* and *Cd7*),[45,46] antigen presentation (*Mgl2*, *Xcr1*, and *Il4i1*),[47–49] and innate immune stress pathways (*Pglyrp2* and *Iapp*) (Figure 6e).[50,51]

Contralateral Nx increases proliferation of $PAX2^+$ tubular progenitors

To investigate the regenerative response of the kidney tubule to Nx after UIRI, we used the conditional Pax2/Confetti

Figure 3 | (continued) (UIRI n = 6; UIRI + Nx n = 6) after UIRI. (**e**) Mean tubular diameter (μm) in control animals (n = 6) and animals euthanized 3 days (n = 5), 7 days (UIRI n = 6; UIRI + Nx n = 7), 21 days (UIRI n = 7; UIRI + Nx n = 9), or 42 days (UIRI n = 6; UIRI + Nx n = 6) after UIRI. (**f**) Density ridgeline plot of all tubular diameters (μm) presented in (**e**). (**g**) Mean tubular counts per total tissue size (mm^{-2}) in cortex (upper panel) and medulla (lower panel), in control animals (n = 6) and animals euthanized 3 days (n = 5), 7 days (UIRI n = 6; UIRI + Nx n = 7), 21 days (UIRI n = 7; UIRI + Nx n = 9), or 42 days (UIRI n = 6; UIRI + Nx n = 6) after UIRI. (**h**) Mean interstitial area per total tissue size (%) in control animals (n = 6) and animals euthanized 3 days (n = 5), 7 days (UIRI n = 6; UIRI + Nx n = 6), 21 days (UIRI n = 7; UIRI + Nx n = 9), or 42 days (UIRI n = 6; UIRI + Nx n = 5) after UIRI. (**i**) Density ridgeline plot of interstitial area per total tissue size (%) presented in (**h**). (**j**) Representative images of Sirius red staining. Bar = 100 μm. (**k**) Histologic quantification of Sirius red staining in control animals (n = 5) and animals euthanized 3 days (n = 6), 7 days (UIRI n = 5; UIRI + Nx n = 6), 21 days (UIRI n = 6; UIRI + Nx n = 7), or 42 days (UIRI n = 6; UIRI + Nx n = 6) after UIRI. (**l**) *Tgfβ* gene expression by quantitative polymerase chain reaction in control animals (n = 6) and animals euthanized 3 days (n = 6), 7 days (UIRI n = 6; UIRI + Nx n = 7), 21 days (UIRI n = 7; UIRI + Nx n = 9), or 42 days (UIRI n = 6; UIRI + Nx n = 6) after UIRI. Data are presented as mean + SD. For ridgelines: plotted dots each represent an individual animal's parameter value, where colors indicate the study group (yellow: UIRI; blue: UIRI + Nx; white: control). Vertical lines indicate distribution means, based on plotted values. Data are from time course study in mice with left renal UIRI for 21 minutes at 34 °C core body temperature. In all UIRI + Nx groups, Nx was performed 3 days after UIRI. Data are presented as mean + SD. *Adjusted *P* (*P*.adj) < 0.05 between groups; #*P*.adj < 0.05 versus control. To optimize viewing of this image, please see the online version of this article at www.kidney-international.org.

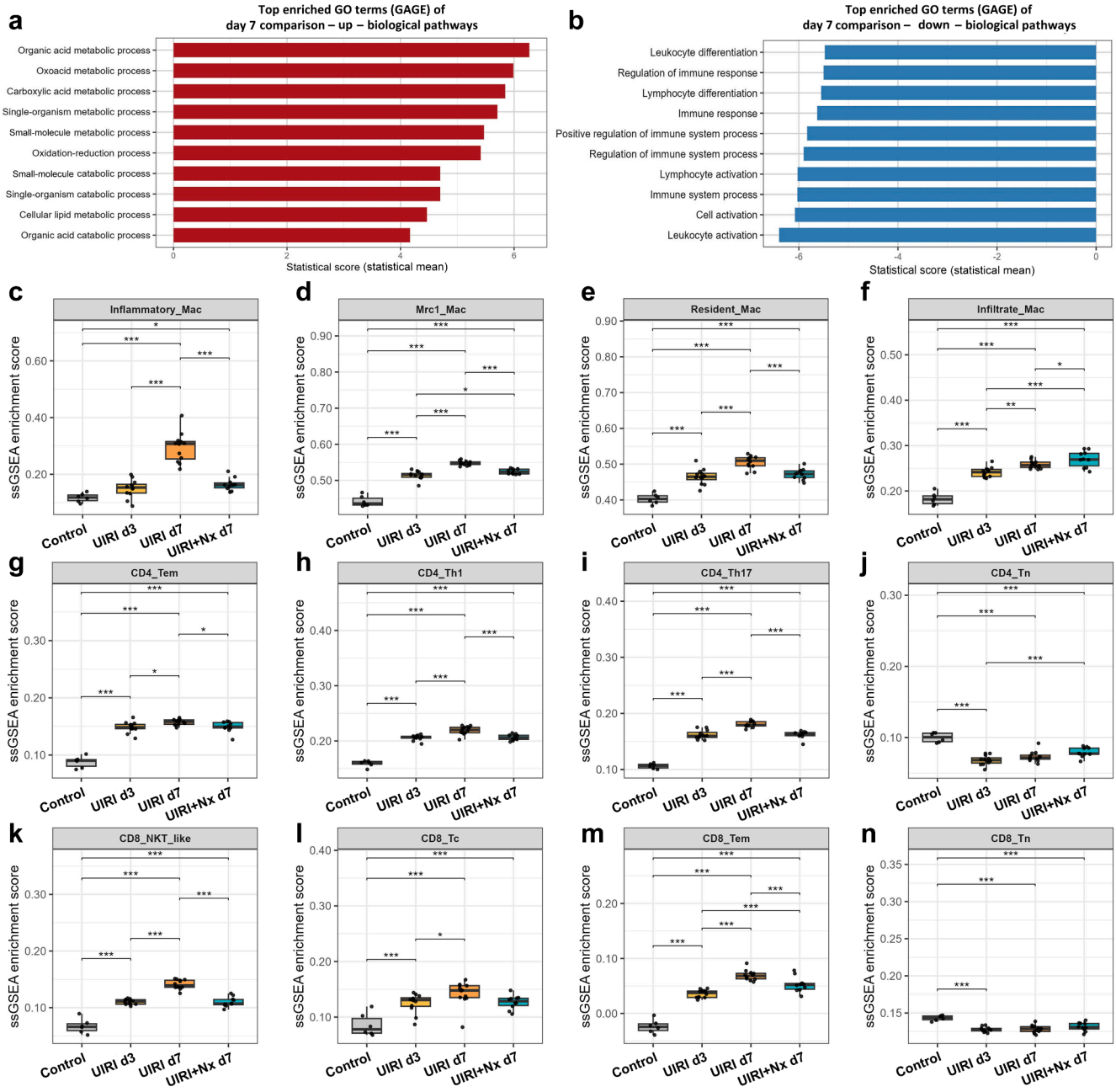


Figure 4 | Nephrectomy (Nx) on day 3 after unilateral ischemia-reperfusion injury (UIRI) reshapes metabolic and inflammatory programs. (**a,b**) Top 10 significant Gene Ontology (GO) enrichment terms linked to significant differentially expressed genes (adjusted *P* [*P*.adj] < 0.05) of the day (d) 7 comparison (i.e., UIRI day 7 vs. UIRI + Nx day 7, with Nx performed on day 3 after UIRI). Results visualized as bar plots (statistical mean per term). Red: positively enriched GO biological pathway terms. Blue: negatively enriched GO biological pathway terms. (**c–n**) Single-sample gene set enrichment analysis (ssGSEA) estimated relative abundances of immune cell subtypes per group. (**c–f**) Macrophages: enrichment scores of macrophages per group. (**g–j**) $CD4^+$ T cells: enrichment scores of $CD4^+$ T cells per group. (**k–n**) $CD8^+$ T cells: enrichment scores of $CD8^+$ T cells per group. Normalized, variance-stabilized counts were used as input for ssGSEA. Box plots show individual enrichment scores ± mean SD. Dots represent individual scores. Within individual graphs, groups are indicated from left to right: gray = controls, yellow = UIRI day 3, orange = UIRI day 7 without Nx, and blue = UIRI + Nx day 7 with Nx performed on day 3. Significance threshold at Benjamini-Hochberg *P*.adj < 0.05. **P*.adj < 0.05, ***P*.adj < 0.01, ****P*.adj < 0.001. CD4, $CD4^+$ T cells; CD4_Tem, $CD4^+$ effector memory T cells; CD4_Th1, $CD4^+$ Th1 T-helper cells type 1; CD4_Th17, $CD4^+$ T-helper cells type 17; CD4_Tn, naive $CD4^+$ T cells; CD8, $CD8^+$ T cells; CD8_NKT_like, $CD8^+$ natural killer T cells; CD8_Tc, $CD8^+$ cytotoxic T cells; CD8_Tem, $CD8^+$ effector memory T cells; CD8_Tn, $CD8^+$ naive T cells; GAGE, Generally Applicable Gene-set Enrichment; Inflammatory_Mac, inflammatory macrophages; Infiltrate_Mac, infiltrating macrophages; Mac, macrophages; Mrc1_Mac, mannose receptor C-type 1 high-expressing macrophages; Resident_Mac, kidney resident macrophages.

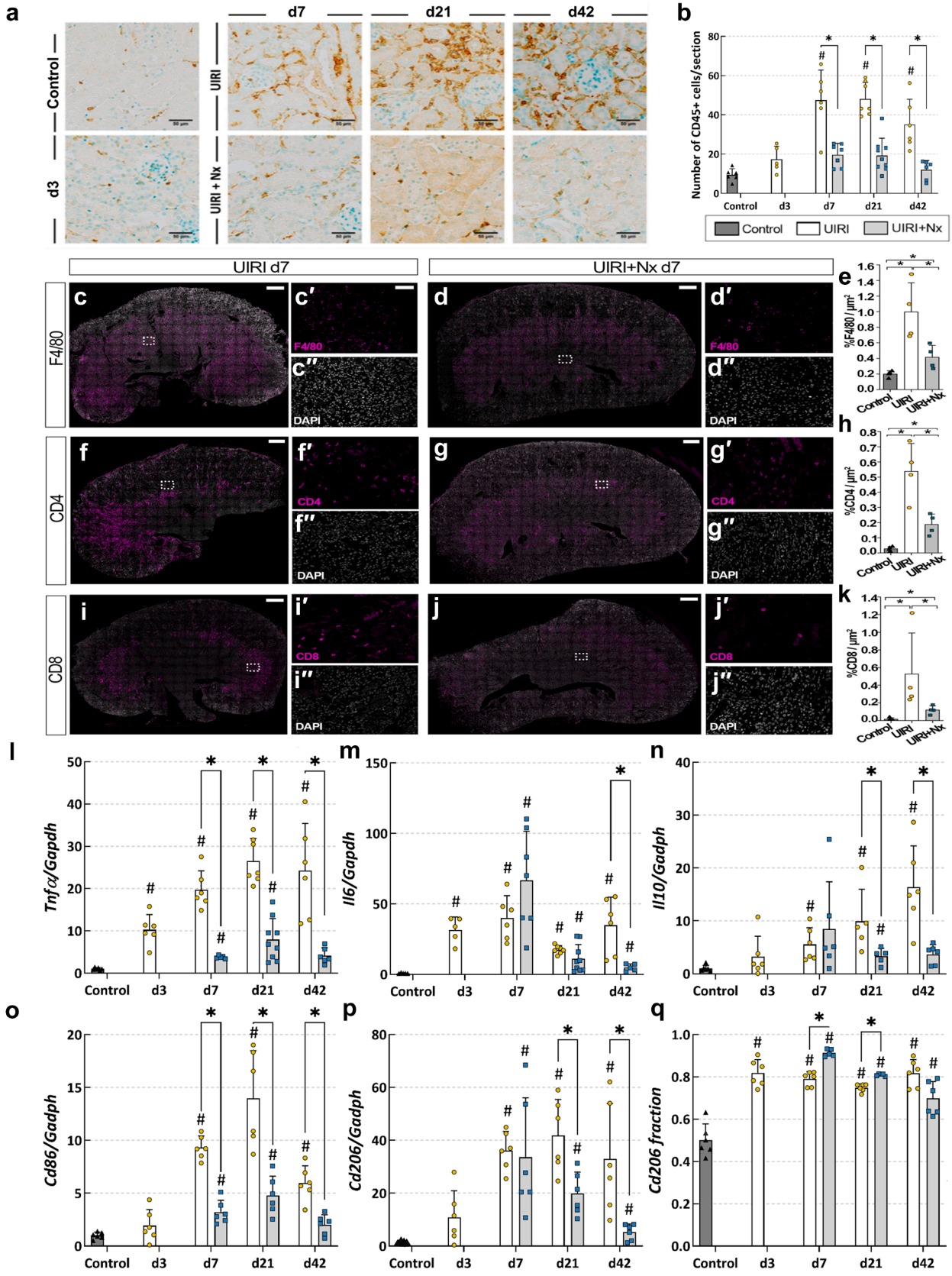


Figure 5 | Nephrectomy (Nx) on day (d) 3 after unilateral ischemia-reperfusion injury (UIRI) attenuates and reshapes the inflammatory response. (**a**) Representative images of CD45 staining. Bar = 100 µm. (**b**) Histologic quantification of CD45 staining in control animals (n = 6) and animals euthanized 3 days (n = 5), 7 days (UIRI n = 6; UIRI + Nx n = 7), 21 days (UIRI n = 7; UIRI + Nx n = 9), or 42 days (UIRI n = 6; UIRI + Nx n = 6) after UIRI. (**c,d**) Sequential scanning of whole kidney section stained for F4/80 in mice on day 7 (continued)

mouse model enabling the lineage tracing of $Pax2^+$ tubular progenitors at 7 and 30 days after UIRI. Following the ischemic insult, the proximal tubules in the outer stripe of outer medulla (OSOM) sustained severe injury, whereas those in the cortex were only mildly affected (Supplementary Results and Supplementary Figure S8A–D). Quantification of $Pax2^+$ tubular progenitors was performed in cortex and OSOM after staining for aquaporin-2 to exclude the collecting ducts (Figure 7a–f and h–m, Supplementary Results, and Supplementary Figure S8E–H). The number of $Pax2^+$ tubular progenitors significantly increased after UIRI and UIRI + Nx in comparison to healthy controls (Supplementary Results and Supplementary Figure S8I and J) with the generation of clones in UIRI and UIRI + Nx on both day 7 (Figure 7a–f, Supplementary Results, and Supplementary Figure S8E and F) and day 30 (Figure 7h–m, Supplementary Results, and Supplementary Figure S8G and H). Accordingly, clone frequency was higher in both UIRI and UIRI + Nx groups on day 7 and day 30 (Figure 7g and n, Supplementary Results, and Supplementary Figure S8K). However, although in the cortex clones consisted of up to 6 cells on day 30 (Supplementary Results and Supplementary Figure S8K), in OSOM they were longer (Figure 7g and n). Remarkably, clone frequency was higher in the UIRI + Nx group than in the UIRI group on day 30 in OSOM (Figure 7n). At this latter time point, we observed a higher percentage of clonogenic $Pax2^+$ tubular progenitors in UIRI + Nx in comparison to UIRI (Figure 7o), resulting in clones that were more numerous and longer (Figure 7p and q). This was confirmed by a significantly higher percentage of new TECs generated by $Pax2^+$ tubular progenitor proliferation in UIRI + Nx compared with UIRI (77.21 ± 34.44 vs. 39.19 ± 12.89; $P = 0.005$) (Figure 7r). No difference in the percentage of lost $Pax2^+$ tubular progenitors between UIRI and UIRI + Nx was observed, suggesting no different survival capacity (Figure 7s). In the cortex, the expansion of $Pax2^+$ tubular progenitors was minimal, resulting in no significant differences between UIRI and UIRI + Nx mice in clone frequency, the percentage of clonogenic cells, or the number of new clones (Supplementary Results and Supplementary Figure S8K–M). Overall, these findings indicated that the greater clonogenic potential observed after Nx is because of an increased involvement of $Pax2^+$ tubular progenitors endowed with the ability to expand clonally in OSOM, the site of injury.

Next, a 3-dimensional analysis was performed in OSOM to analyze the actual clone length in both groups. This showed single clones consisting of up to 146 cells regenerating long tubule segments (Figure 7t–w and Supplementary Movies S1 and S2). Clonogenic $Pax2^+$ tubular progenitor cells and the total number of clones increased in the UIRI + Nx compared with UIRI (Figure 7x and y, Supplementary Results, and Supplementary Figure S8N), confirming the 2-dimensional analysis. Collectively, Nx after UIRI stimulates $Pax2^+$ tubular progenitors to generate more numerous and longer clones than UIRI alone.

Nx attenuates TEC polyploidization

Polyploidization of TECs is another major response that influences AKI outcomes.[10] To investigate the effect of Nx thereon, we used the inducible Pax8/FUCCI2aR mice model enabling the combined flow cytometric analysis of TEC DNA content with detection of the cell cycle–dependent FUCCI2aR fluorescent proteins (mCherry, red; and mVenus, green). Fluorescence-activated cell sorting analysis revealed a peak of polyploid TECs ($mCherry^+$, $mCherry^+/mVenus^+$ with a DNA content ≥4C or $mVenus^+$ with a DNA content ≥8C) on day 3 after UIRI, showing that polyploid TECs have already been generated when Nx was performed (Figure 8a, b, and g). Although the overall percentage of polyploid TECs was not significantly different between UIRI and UIRI + Nx on day 7 (4 days after Nx) or day 30 (27 days after Nx) (Figure 6g), a distinct difference in the progression of polyploid TECs between the 2 groups was observed. On day 30, polyploid TECs with octaploid or higher DNA content were significantly more prevalent in the UIRI group compared with those observed in the UIRI + Nx group (Figure 8d, f, and h), suggesting that UIRI triggered

Figure 5 | (continued) (UIRI n = 4; UIRI + Nx n = 4). (**c′–d′′**) Higher magnification of the boxed area. 4′,6-Diamidino-2-phenylindole (DAPI) counterstains nuclei. Bars = 500 μm. (**e**) Quantification of $F4/80^+$ cells by digital morphometry. (**f,g**) Sequential scanning of whole kidney section stained for CD4 in mice on day 7 (UIRI n = 4; UIRI + Nx n = 4). (**f′–g′′**) Higher magnification of the boxed area. DAPI counterstains nuclei. Bars = 500 μm. (**h**) Quantification of $CD4^+$ cells by digital morphometry. (**i,j**) Sequential scanning of whole kidney section stained for in mice on day 7 (UIRI n = 4; UIRI + Nx n = 4). (**i′–j′′**) Higher magnification of the boxed area. DAPI counterstains nuclei. Bars = 500 μm. (**k**) Quantification of $CD8^+$ cells by digital morphometry. (**l**) *Tnf-α* gene expression by quantitative polymerase chain reaction (qPCR) in control animals (n = 6) and animals euthanized 3 days (n = 6), 7 days (UIRI n = 6; UIRI + Nx n = 5), 21 days (UIRI n = 7; UIRI + Nx n = 9), or 42 days (UIRI n = 6; UIRI + Nx n = 6) after UIRI. (**m**) *Il-6* gene expression by qPCR in control animals (n = 5) and animals euthanized 3 days (n = 5), 7 days (UIRI n = 6; UIRI + Nx n = 7), 21 days (UIRI n = 7; UIRI + Nx n = 9), or 42 days (UIRI n = 6; UIRI + Nx n = 5) after UIRI. (**n**) *Il-10* gene expression by qPCR in control animals (n = 6) and animals euthanized 3 days (n = 6), 7 days (UIRI n = 6; UIRI + Nx n = 6), 21 days (UIRI n = 5; UIRI + Nx n = 5), or 42 days (UIRI n = 6; UIRI + Nx n = 6) after UIRI. (**o**) *Cd86* gene expression by qPCR in control animals (n = 6) and animals euthanized 3 days (n = 6), 7 days (UIRI n = 6; UIRI + Nx n = 6), 21 days (UIRI n = 6; UIRI + Nx n = 6), or 42 days (UIRI n = 6; UIRI + Nx n = 6) after UIRI. (**p**) *Cd206* (*Mrc1*) gene expression by qPCR in control animals (n = 6) and animals euthanized 3 days (n = 6), 7 days (UIRI n = 6; UIRI + Nx n = 6), 21 days (UIRI n = 6; UIRI + Nx n = 6), or 42 days (UIRI n = 6; UIRI + Nx n = 6) after UIRI. (**q**) Fraction of *Cd206* (*Mrc1*) expression by formula: [*Cd206* fraction = *Cd206* fold change/(*Cd86* fold change + *Cd206* fold change)]. Data are given for control animals (n = 6) and animals euthanized 3 days (n = 6), 7 days (UIRI n = 6; UIRI + Nx n = 5), 21 days (UIRI n = 6; UIRI + Nx n = 5), or 42 days (UIRI n = 6; UIRI + Nx n = 6) after UIRI. In all UIRI + Nx groups, Nx was performed 3 days after UIRI. Data are presented as mean + SD. Significance at $*P < 0.05$ between groups; $\#P < 0.05$ versus control. To optimize viewing of this image, please see the online version of this article at www.kidney-international.org.

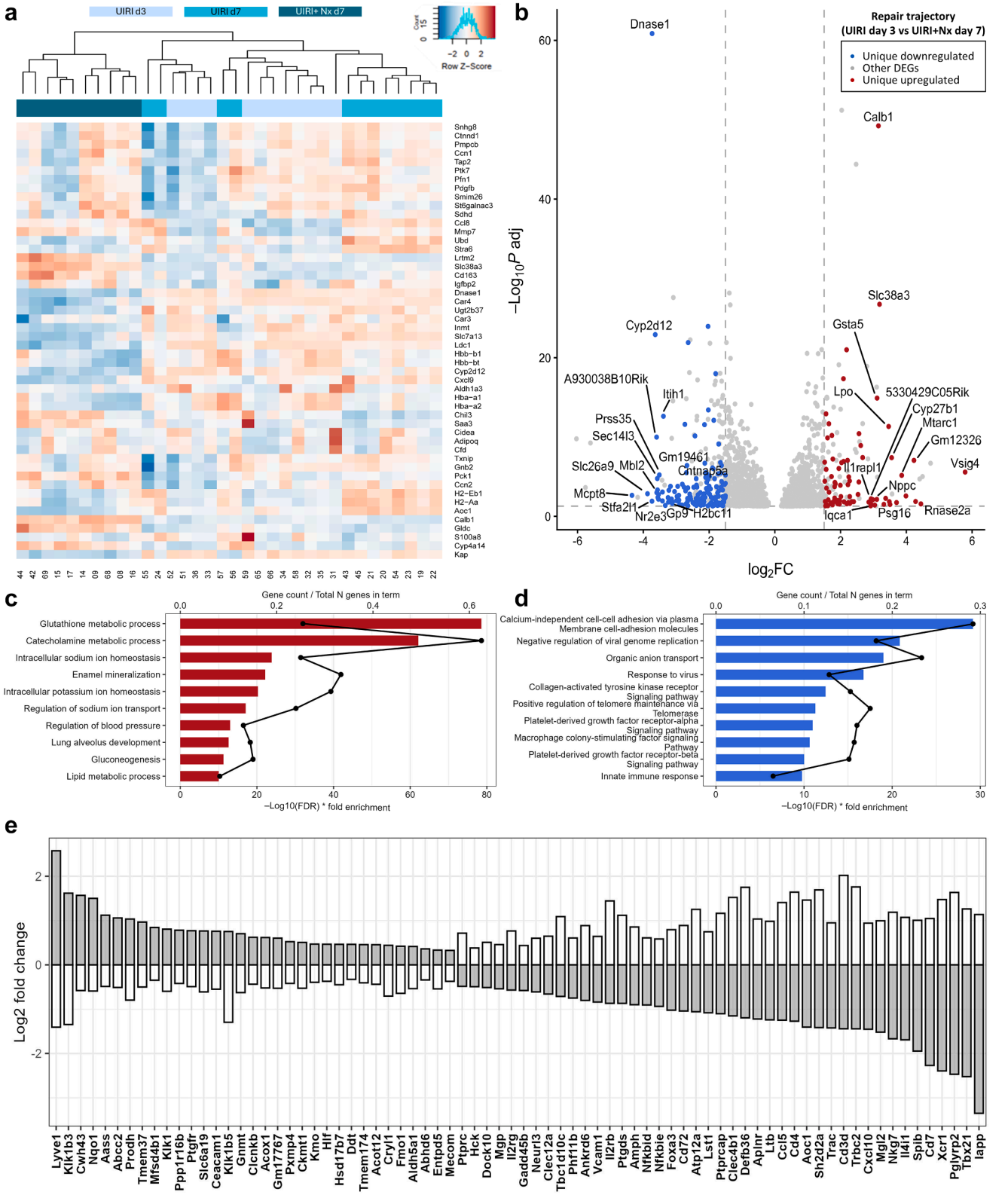


Figure 6| Transcriptomics reveals metabolic reprogramming and repair-associated gene sets. (**a**) Heat map of variance-stabilized, normalized, and scaled gene expression across samples for the 50 most variable genes. Each column represents a single sample, and each row represents a gene. Samples are of 2 independent studies combined (Supplementary Table S2): unilateral ischemia-reperfusion injury (UIRI) day (d) 3 (n = 12), UIRI d7 (n = 12), and UIRI + nephrectomy (Nx) d7 (n = 10). (**b**) Volcano plot of significant differentially expressed genes (DEGs) of the repair trajectory (i.e., UIRI day 3 vs. UIRI + Nx day 7). Red and blue colored points indicate unique upregulated and downregulated DEGs of this trajectory, respectively, of which the top ranked are in bold. Gray points indicate either (continued)

continuous reentrance of the cell cycle acquiring additional sets of chromosomes over time. In contrast, performing Nx 3 days after UIRI halted the polyploidization progression. Indeed, the percentage of octaploid TECs did not increase between days 7 and 30 after injury and was significantly lower compared with the UIRI group by day 30 (Figure 8h). In line with this the percentage of cycling octaploid TECs ($mCherry^+/mVenus^+$ with a DNA content >4C and $mVenus^+$ with a DNA content ≥8C) was significantly reduced in the UIRI + Nx group on day 30 (Figure 8i). Collectively, Nx following UIRI prevents ongoing polyploid TEC formation.

DISCUSSION

Averting transition to CKD and promoting kidney regeneration remain important therapeutic goals in AKI. Intriguingly, removal of the contralateral kidney (Nx) after UIRI can improve kidney outcome. Here, we report that full functional recovery from UIRI in mice and rats can be achieved when Nx is performed early (i.e., on day 3 after ischemic injury), whereas Nx on later time points had no significant effects on the progression toward CKD, suggesting an optimal "intervention" window shortly after AKI. On the cellular level, Nx attenuated and reshaped the inflammatory response and enhanced kidney recovery by stimulating the proliferation of tubular progenitors while inhibiting continuous TEC polyploidization. At the transcriptomic level, an Nx-induced prorepair signature was identified.

The timing of Nx is an important determinant of AKI recovery outcomes, affecting not only kidney function and structure but also survival. Indeed, a previous study showed that when Nx is performed immediately (on days 0 and 1) after UIRI in rats, the mortality rates were high (80% and 75%, respectively), with animals dying within 2 to 3 days after Nx, suggesting death by kidney insufficiency.[52] With increasing Nx delay (days 2, 4, and 14), mortality rates decreased (to 40%, 8%, and 15%, respectively), indicating that several days of recovery are required to improve post-Nx survival.[52] However, despite an improved survival, late Nx failed to prevent fibrosis and restore kidney function.[52] Remarkably, only when Nx was performed on day 2, albeit with a 40% mortality, nearly normal kidney function recovery was noted in the surviving rats.[52] Similarly, in murine models where Nx was delayed for 7 days, normal function was never regained, and fibrosis developed.[25,53,54] Using rat and murine UIRI models, we here demonstrated that Nx on day 3 resulted in full functional recovery without mortality and restored kidney structure, albeit with morphometric adaptation.

Cellular insight into how Nx induces structural and functional kidney recovery, attenuating fibrosis, is rudimental. The fundamental question as to whether tubular regeneration is involved has not been adequately answered. Previous studies revealed increases in kidney DNA content, bromodeoxyuridine or 3H-thymidine uptake, presence of chromosomal mitotic figures, and expression of conventional cell cycle markers as indicators of proliferation.[13,55–57] However, new insights in the response of surviving TECs after injury (i.e., progenitor mitosis vs. polyploidy of differentiated TECs) revealed the incapacity of these indicators to conclude on whether and to what extent Nx-induced recovery goes along with actual proliferation. By tracking proliferation of individual tubular progenitors in transgenic Pax2/Confetti mice, we demonstrated a significant increase in $Pax2^+$ tubular progenitor clonal expansion in both UIRI and UIRI + Nx groups, which was lower in the cortex than in the OSOM, in agreement with the fact that cortex sustained milder injury in our ischemic model. More importantly, where $Pax2^+$ tubular progenitor-driven regeneration occurs, we demonstrated that Nx stimulates a higher number of $Pax2^+$ tubular progenitors to generate more numerous and longer clones in comparison to spontaneous repair after UIRI. Hence, Nx after UIRI boosts tubular regeneration.

Insight into why day 3 after AKI is a critical time point for survival might be provided by our present and past observations on TEC polyploidization.[9,10] In FUCCI2aR mice, we reconfirmed a robust polyploid response immediately after the ischemic insult, aligning with a time-course analysis where polyploidy peaked at day 3 after AKI.[10] The increased polyploidy has previously been shown to be essential for rapid functional recovery in the initial days after injury, ensuring AKI survival.[9,10] Interestingly, analyses of TEC polyploidy in Pax8/FUCCI2aR mice on Nx at day 3 clearly showed that Nx mitigated polyploid TECs to continue reentering the cell cycle and acquire multiple DNA copies. This suggests that when Nx is performed too early after injury (before day 2), insufficient TEC polyploidization occurred to be lifesaving, likely explaining the previously observed higher mortality rates with such early Nx.[10,52] Overall, although the optimal postinjury time point for Nx may vary with injury severity and polyploid response, in our studies, a minimal delay of 3 days emerged as rather critical.

As continuous TEC polyploidization after UIRI has been shown to be responsible for senescence and interstitial

Figure 6 | (continued) nonsignificant genes (between the vertical dashed lines) or nonunique DEGs (outside the vertical dashed lines). Thresholds are set at –log10(adjusted *P* [*P*.adj]) < 0.05 and at and absolute log2foldchange (FC) of > 1.5 (gray lines). (**c,d**) Functional annotation analysis via the Database for Annotation, Visualization, and Integrated Discovery (DAVID) of unique genes of the repair trajectory (i.e., UIRI day 3 vs. UIRI + Nx day 7). Bar graphs showing the top 10 significant Gene Ontology biological process terms enriched for the (**c**) upregulated (red bars) and (**d**) downregulated (blue bars) unique DEGs with gene ratio of DEGs involved (trendline). Bars are ordered according to rank score (–log10[false discovery rate {FDR}] * fold enrichment). Significance at $P < 0.05$ and FDR < 0.05. (**e**) Bar graph depicting genes with significant (*P*.adj < 0.05) contraregulated log2foldchanges between the injury (i.e., UIRI day 3 vs. UIRI day 7) and repair trajectories (i.e., UIRI day 3 vs. UIRI + Nx day 7). White: log2foldchanges in the injury trajectory. Gray: log2foldchanges in the repair trajectory. Data are from 2 time course studies in mice with left renal UIRI for 21 minutes at 34 °C or 36 °C core body temperature. In all UIRI + Nx groups, Nx was performed 3 days after UIRI.

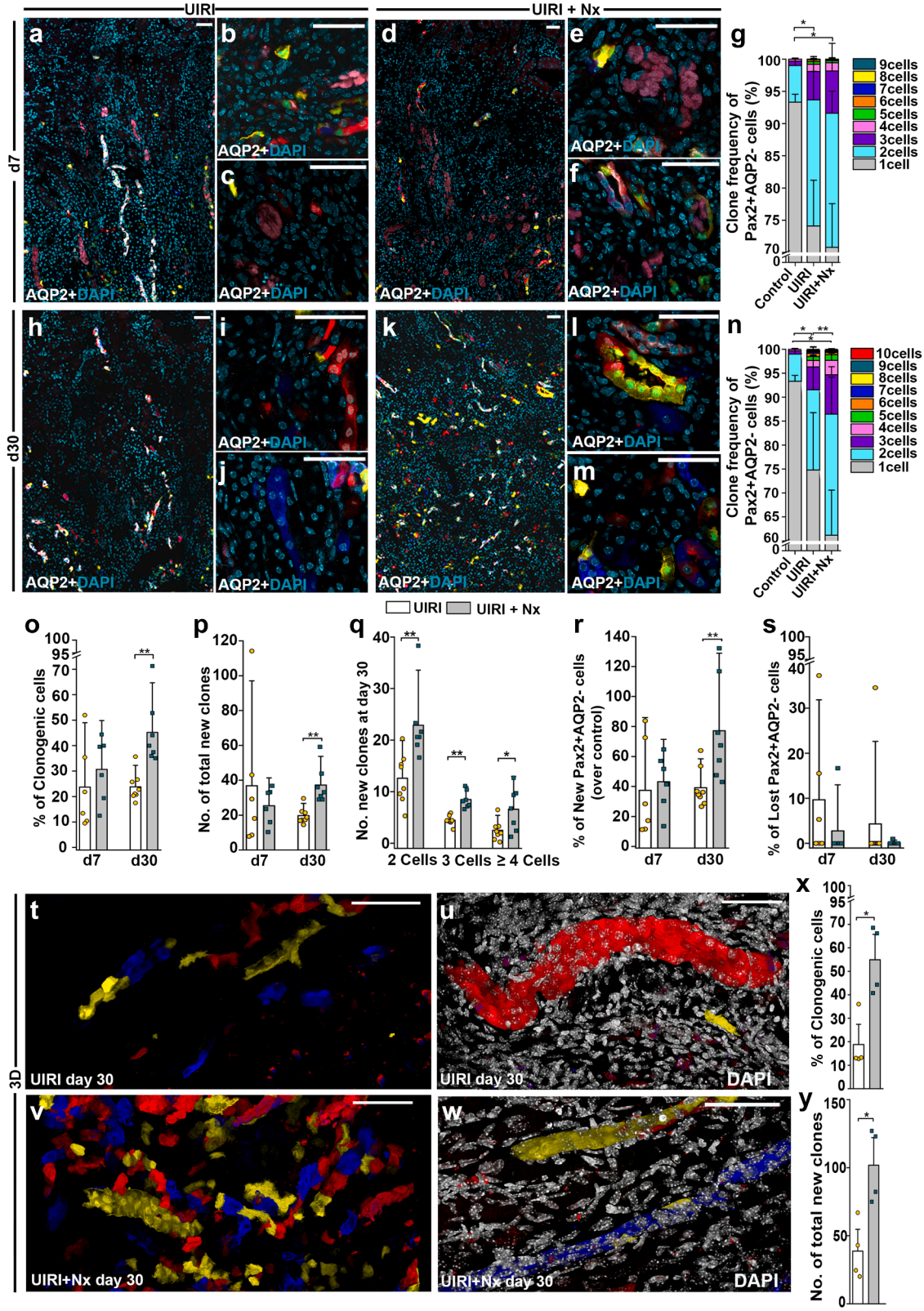


Figure 7 | Nephrectomy (Nx) after unilateral ischemia-reperfusion injury (UIRI) recruits more Pax2$^+$ tubular progenitor cells endowed with a higher clonogenic ability. (**a**) Representative image of Pax2$^+$/Confetti mice kidneys in outer stripe of outer medulla (OSOM) on day (d) 7 after UIRI (n = 6). Aquaporin-2 (AQP2) staining is white. 4′,6-Diamidino-2-phenylindole (DAPI) counterstains nuclei. (**b,c**) Higher magnification of Pax2$^+$/Confetti mice kidneys in OSOM on day 7 after UIRI. AQP2 staining is white. DAPI counterstains nuclei. (**d**) Representative image of Pax2$^+$/Confetti mice kidneys in OSOM on UIRI + Nx day 7 (n = 6). Nx was performed on day 3 after UIRI. AQP2 staining is white. DAPI counterstains nuclei. (**e,f**) Higher magnification of Pax2$^+$/Confetti mice kidneys in OSOM on UIRI + Nx (continued)

fibrosis,[11] its reduction on Nx would explain the prevention of the AKI-to-CKD transition.[10] One contributing pathway may be transforming growth factor (TGF)-β, which promotes and self-reinforces polyploidization.[11] We found TGF-β expression to be reduced after Nx, consistent with reports showing a rapid (≤24-hour) decline in TGF-β in remnant kidneys, independent of whether these were healthy or injured.[25,58] In addition, polyploidization may also be reduced as enhanced epithelial regeneration progressively restores structure and function, thereby diminishing the need for this adaptive compensatory mechanism. Furthermore, it is remarkable that Nx exerts apparently opposing effects on cell cycle behavior depending on the phenotype of the proximal tubular cells (i.e., boosting proliferation of tubular progenitors while attenuating continuous polyploidization of TECs). Although it remains to be defined whether and how these 2 responses could be mechanistically related, it is clear that Nx induces an overall benign shift in the tubular injury-response programs.

Previous work showed that Nx reduces kidney inflammation, including macrophage recruitment, but effects on macrophage polarization and broader immune-cell dynamics have remained unclear.[25,28,29] In our analysis, transcriptomics, quantitative PCR, and immunostaining confirmed a highly suppressed immune response after Nx, with reductions in macrophages as well as in $CD4^+$ and $CD8^+$ T cells and dendritic cells. Moreover, we found that Nx induced a rapid decline in proinflammatory macrophages, whereas prorepair phenotypes persisted longer before eventually falling below levels observed in the natural AKI-to-CKD trajectory. Thus, early Nx attenuates and reshapes the inflammatory response toward a more repair-permissive profile. The early suppression of leukocyte infiltration further suggests that Nx at day 3 primarily acts by reducing inflammatory cues originating from the injured epithelium. Remarkably, as observed in our rat study, late Nx also suppressed immune cell infiltration, whereas fibrosis and atrophy were not averted. This suggests that once certain maladaptive epithelial programs are established, dampening immune infiltration alone might not be sufficient to avert demise.

At the gene level, transcriptomic analysis demonstrates that Nx redirects the injury response toward a repair program characterized by improved cellular stress handling, restored transport functions, and rebalanced energy homeostasis. This shift is captured by a distinct gene set uniquely associated with Nx-induced repair, as well as a set of contraregulated genes that define the transcriptional switch between maladaptive and successful repair. Identification of a robust core set of Nx-responsive genes offers concrete mechanistic entry points. Several of these genes align with known renoprotective pathways, whereas others point to less explored biology in kidney repair. For example, consistent Nx-induced upregulation of Cyp27b1 (encoding 1-α-hydroxylase) raises the possibility that local vitamin D activation and pleiotropic signaling are involved beyond its role in calcium-phosphate homeostasis. This is supported by prior studies demonstrating renoprotective and pro-reparative effects of vitamin D in experimental kidney injury models,[59–62] as well as by its ability to suppress Th1 and Th17 cell function,[63–66] which is in accordance with the suppressed CD4_Th1 and CD4_Th17 signatures noted in our single-sample gene set enrichment analysis.

There are several limitations to this work. First, Nx is obviously not a directly translatable intervention. However, by unraveling its cellular mechanisms, we can learn how nature achieves such an effective multifaceted repair response, inspiring the design of novel therapeutic strategies. Second, although our transcriptomic analysis identified genes robustly associated with the Nx-induced prorepair shift, their functional causality, hierarchy, and cell type specificity remain to be established. Nonetheless, the identified gene sets provide a robust rational framework to prioritize candidates for future mechanistic studies. Third, our study does not provide insight into involved systemic signals. It is also not known whether the injured tissue becomes less susceptible to Nx-induced signals, or whether Nx-induced signals become less potent with time. Nonetheless, we identified

Figure 7 | (continued) day 7. AQP2 staining is white. DAPI counterstains nuclei. (**g**) Clone frequency analysis of $Pax2^+AQP2^-$ tubular progenitor cells on day 7; control versus UIRI day 7 $^*P = 0.02$; control versus UIRI + Nx day 7 $^*P = 0.02$. (**h**) Representative image of $Pax2^+$/Confetti mice kidneys in OSOM on day 30 after UIRI (n = 8). AQP2 staining is white. DAPI counterstains nuclei. (**i,j**) Higher magnification of $Pax2^+$/Confetti mice kidneys in OSOM on day 30 after UIRI. AQP2 staining is white. DAPI counterstains nuclei. (**k**) Representative image of $Pax2^+$/Confetti mice kidneys in OSOM on UIRI + Nx day 30 (n = 7). AQP2 staining is white. DAPI counterstains nuclei. (**l,m**) Higher magnification of $Pax2^+$/Confetti mice kidneys in OSOM on UIRI + Nx day 30. AQP2 staining is white. DAPI counterstains nuclei. (**n**) Clone frequency analysis of $Pax2^+AQP2^-$ tubular progenitor cells on day 30; control versus UIRI day 30 $^*P = 0.012$; control versus UIRI + Nx day 30 $^*P = 0.016$; UIRI day 30 versus UIRI + Nx day 30 $^*P = 0.02$. (**o**) Percentage of $Pax2^+$ clonogenic cells; UIRI day 30 versus UIRI + Nx day 30 $^{**}P = 0.0006$. (**p**) Number of total new clones; UIRI day 30 versus UIRI + Nx day 30 $^{**}P = 0.001$. (**q**) Number of new clones on day 30; UIRI day 30 versus UIRI + Nx day 30, 2 cells $^{**}P = 0.001$; UIRI day 30 versus UIRI + Nx day 30, 3 cells $^{**}P = 0.0003$; UIRI day 30 versus UIRI + Nx day 30, ≥4 cells $^*P = 0.04$. (**r**) Percentage of new $Pax2^+AQP2^-$ tubular progenitor cells; UIRI day 30 versus UIRI + Nx day 30 $^{**}P = 0.005$. (**s**) Percentage of lost $Pax2^+AQP2^-$ tubular progenitor cells. (**t,u**) Three-dimensional (3D) reconstruction of single-colored clones in Pax2/Confetti mice on day 30 after UIRI (n = 4). DAPI counterstains nuclei (white). (**v,w**) 3D reconstruction of single-colored clones in Pax2/Confetti mice on UIRI + Nx day 30 (n = 4). DAPI counterstains nuclei (white). (**x**) Percentage of $Pax2^+$ clonogenic cells in 3D analysis; UIRI day 30 versus UIRI + Nx day 30 $^*P = 0.02$. (**y**) Number of total new clones in 3D analysis; UIRI day 30 versus UIRI + Nx day 30 $^*P = 0.02$. In all UIRI + Nx groups, Nx was performed 3 days after UIRI. Data are presented as mean + SD. Bars = 50 μm. To optimize viewing of this image, please see the online version of this article at www.kidney-international.org.

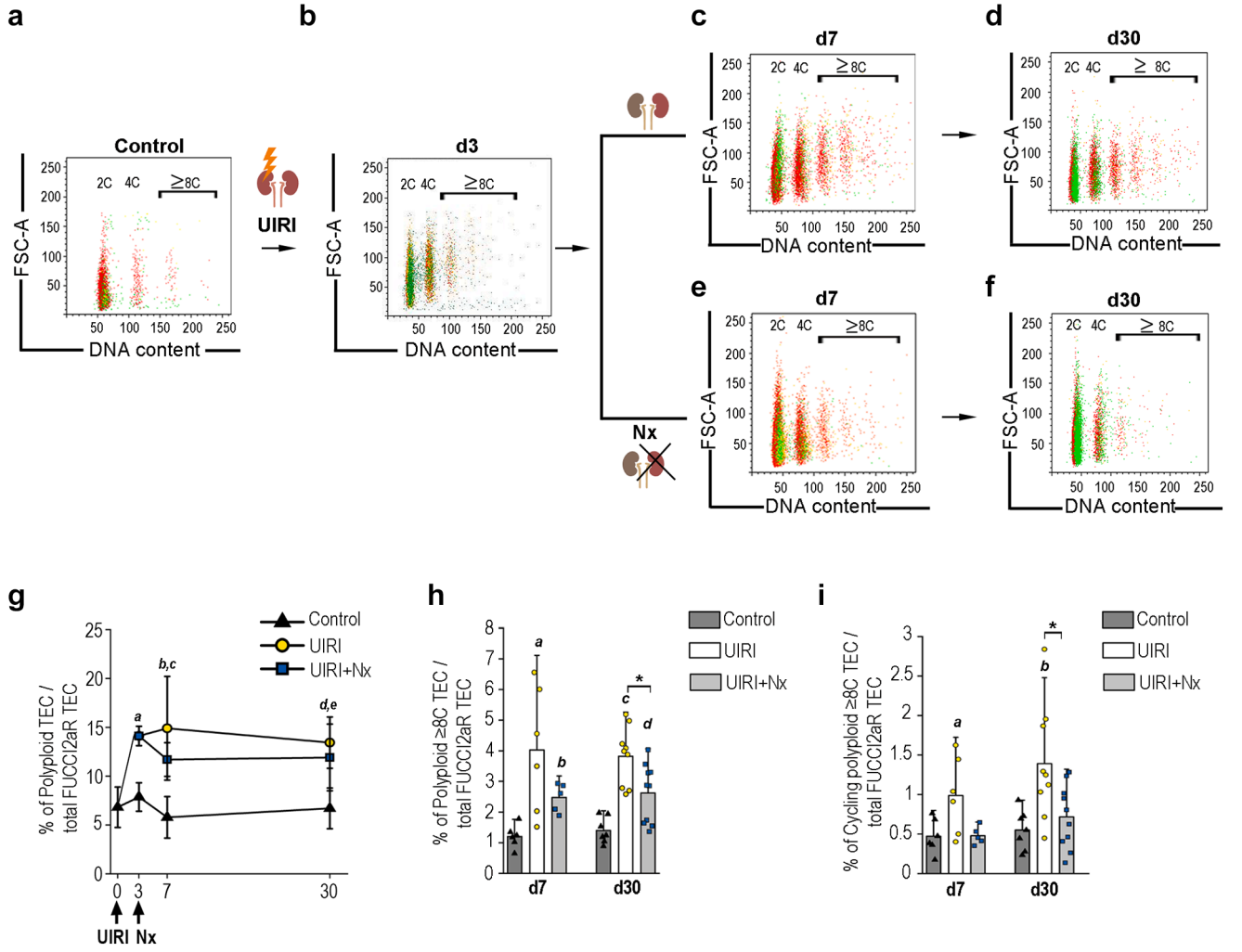


Figure 8 | Nephrectomy (Nx) after unilateral ischemia-reperfusion injury (UIRI) attenuates ongoing polyploidization of tubular epithelial cells (TECs). (**a**) Representative fluorescence-activated cell sorting (FACS) plot of healthy Pax8/FUCCI2aR on day (d) 0 (n = 6). (**b**) Representative FACS plot of Pax8/FUCCI2aR on day 3 after UIRI (n = 5). (**c**) Representative FACS plot of Pax8/FUCCI2aR on day 7 after UIRI (n = 6). (**d**) Representative FACS plot of Pax8/FUCCI2aR on day 30 after UIRI (n = 9). (**e**) Representative FACS plot of Pax8/FUCCI2aR on UIRI + Nx day 7 (n = 5). (**f**) Representative FACS plot of Pax8/FUCCI2aR on UIRI + Nx day 30 (n = 10). All the plots show diploid (2C), tetraploid (4C), and octaploid or greater (≥8C) TECs. Colors match the FUCCI2aR reporter. (**g**) Percentage of total polyploid TECs. [a]Control day 3 (n = 5) versus UIRI day 3 (n = 4) $P = 0.01$; [b]Control day 7 (n = 6) versus UIRI day 7 (n = 6) $P = 0.004$; [c]Control day 7 (n = 6) versus UIRI + Nx day 7 (n = 5) $P = 0.004$; [d]Control day 30 (n = 7) versus UIRI day 30 (n = 9) $P = 0.0001$; [e]Control day 30 (n = 7) versus UIRI + Nx day 30 (n = 10) $P = 0.004$. (**h**) Percentage of polyploid 8C TECs. [a]Control day 7 versus UIRI day 7 $P = 0.004$. [b]Control day 7 versus UIRI + Nx day 7 $P = 0.004$. [c]Control day 30 versus UIRI day 30 $P = 0.0001$. [d]Control day 30 versus UIRI + Nx day 30 $P = 0.009$. *$P = 0.04$. (**i**) Percentage of cycling polyploid 8C TECs. [a]Control day 7 versus UIRI day 7 $P = 0.04$. [b]Control day 30 versus UIRI day 30 $P = 0.005$. *$P = 0.02$. In all UIRI + Nx groups, Nx was performed 3 days after UIRI. Data are presented as mean + SD. FSC, forward scatter.

relevant dynamics of the model and a time frame allowing such investigations. A thorough understanding of tissue-level processes will ultimately support more targeted identification of such upstream signals. Fourth, our study does not provide information on effects beyond 9 weeks of Nx-induced recovery. Experimental treatments as well as spontaneous repair responses often have inherent adverse effects. Peired *et al.* demonstrated that Pax2^{+} tubular progenitor stimulation as well as activation of injury-related pathways that drive proliferation can cause papillary cell carcinoma.[2,3] Tod *et al.* showed that injured kidneys, which were functionally only partially rescued by Nx performed on day 7 after UIRI, developed euthanasia-requiring end-stage kidney disease at 140 days.[25] For Nx-rescued kidneys with full functional recovery (as in our study with Nx on day 3), it remains to be determined to what extent progression to CKD and/or progenitor carcinogenicity is delayed or avoided on the really long-term.

In summary, our study identified a window of opportunity for intervention after AKI that leads to full functional recovery driven by inherent mechanisms. We demonstrate that Nx-induced recovery is associated with an attenuated and remodeled inflammatory response, a stimulated tubular progenitor proliferation, and an inhibition of polyploid TEC

build-up, thereby promoting kidney repair. This study not only reinforces the value of the Nx model for elucidating the kidney's inherent regenerative capacity but also highlights its potential to identify the most upstream signaling events that drive repair.

DISCLOSURE

All the authors declared no competing interests.

DATA STATEMENT

The transcriptomics data supporting the findings of this study are openly available in the National Center for Biotechnology Information's Gene Expression Omnibus repository at https://www.ncbi.nlm.nih.gov/geo/, with accession number GSE268009.

FUNDING

This project has received funding from the Fund of Scientific Research-Flanders (FWO, No. G0A8413N), TOP-BOF research grant University of Antwerp (grant No. 32254), KP-BOF grants University of Antwerp (grant No. 34737 and No. 41504), and DOCPRO4-BOF (fellowship EVC, grant No. 47097), all allocated to BAV. PR is supported by the European Research Council (ERC) under the European Union's Horizon 2020 research and innovation program (grant agreement No. 648274). C-CA was supported by an EMBO short-term fellowship (reference No. 7120), Carlos Martínez-Salgado, and Fransisco J. López-Hernandez. BAV is thankful for hands-on technical training for determination of glomerular filtration rate in conscious rat/mice by transcutaneous measurement provided by Zentrum für Medizinische Forschung (University Heidelberg, Dr. Gretz laboratory, Manheim, Germany). BAV is thankful to the Wellcome Trust, EMBO, and EMBL-EBI for selection to bioinformatic and transcriptomic analysis courses. We are grateful for the excellent technical assistance of Nathalie Le Clef and Hilde Geryl during murine surgery, Esther Bartholomeus during RNA sequencing, and Jana Baues during quantitative polymerase chain reaction. PB is supported by the German Research Foundation (project identifier No. 322900939, No. 445703531, and CRU5011), European Research Council (ERC consolidator grant No. 101001791), the Federal Ministries of Education and Research (BMBF, No. STOP-FSGS-01GM2202C) and Health (Deep Liver, No. ZMVI1-2520DAT111), and the Innovation Fund of the Federal Joint Committee (Transplant.KI, No. 01VSF21048).

Supplementary material is available online at www.kidney-international.org.

REFERENCES

1. Brown JR, Rezaee ME, Marshall EJ, et al. Hospital mortality in the United States following acute kidney injury. *Biomed Res Int*. 2016;2016:4278579.
2. Peired AJ, Lazzeri E, Guzzi F, et al. From kidney injury to kidney cancer. *Kidney Int*. 2021;100:55–66.
3. Peired AJ, Antonelli G, Angelotti ML, et al. Acute kidney injury promotes development of papillary renal cell adenoma and carcinoma from renal progenitor cells. *Sci Transl Med*. 2020;12:eaaw6003.
4. Zager RA, Johnson ACM, Becker K. Acute unilateral ischemic renal injury induces progressive renal inflammation, lipid accumulation, histone modification, and "end-stage" kidney disease. *Am J Physiol Renal Physiol*. 2011;301:F1334–F1345.
5. Zuk A, Bonventre JV. Recent advances in acute kidney injury and its consequences and impact on chronic kidney disease. *Curr Opin Nephrol Hypertens*. 2019;28:397–405.
6. Lazzeri E, Angelotti ML, Peired A, et al. Endocycle-related tubular cell hypertrophy and progenitor proliferation recover renal function after acute kidney injury. *Nat Commun*. 2018;9:1344.
7. Kramann R, Kusaba T, Humphreys BD. Who regenerates the kidney tubule? *Nephrol Dial Transplant*. 2015;30:903–910.
8. Kusaba T, Lalli M, Kramann R, et al. Differentiated kidney epithelial cells repair injured proximal tubule. *Proc Natl Acad Sci U S A*. 2014;111:1527–1532.
9. Lazzeri E, Angelotti ML, Conte C, et al. Surviving acute organ failure: cell polyploidization and progenitor proliferation. *Trends Mol Med*. 2019;25:366–381.
10. De Chiara L, Conte C, Semeraro R, et al. Tubular cell polyploidy protects from lethal acute kidney injury but promotes consequent chronic kidney disease. *Nat Commun*. 2022;13:5805.
11. De Chiara L, Semeraro R, Mazzinghi B, et al. Polyploid tubular cells initiate a TGF-β1 controlled loop that sustains polyploidization and fibrosis after acute kidney injury. *Am J Physiol Cell Physiol*. 2023;325:C849–C861.
12. Guzzi F, Cirillo L, Roperto RM, et al. Molecular mechanisms of the acute kidney injury to chronic kidney disease transition: an updated view. *Int J Mol Sci*. 2019;20:4941.
13. Yang L, Besschetnova TY, Brooks CR, et al. Epithelial cell cycle arrest in G2/M mediates kidney fibrosis after injury. *Nat Med*. 2010;16:535–543.
14. Derks W, Bergmann O. Polyploidy in cardiomyocytes: roadblock to heart regeneration? *Circ Res*. 2020;126:552–565.
15. Gentric G, Desdouets C. Liver polyploidy: Dr Jekyll or Mr Hide? *Oncotarget*. 2015;6:8430.
16. González-Rosa JM, Sharpe M, Field D, et al. Myocardial polyploidization creates a barrier to heart regeneration in zebrafish. *Dev Cell*. 2018;44:433–446.e7.
17. Matsumoto T, Wakefield L, Tarlow BD, et al. *In vivo* lineage tracing of polyploid hepatocytes reveals extensive proliferation during liver regeneration. *Cell Stem Cell*. 2020;26:34–47.e3.
18. Weng A, Herrerias MM, Watanabe S, et al. Lung injury induces alveolar type 2 cell hypertrophy and polyploidy with implications for repair and regeneration. *Am J Respir Cell Mol Biol*. 2022;66:564–576.
19. Zemans RL. Polyploidy in lung regeneration: double trouble or dynamic duo? *Am J Respir Cell Mol Biol*. 2022;66:481–483.
20. Hinman F. Renal counterbalance - an experimental and clinical study with reference to the significance of disuse atrophy. *J Urol*. 1922;9.
21. Hinman F. Experimental hydronephrosis—repair following uretero cystoneostomy in white rats with complete ureteral obstruction. *J Urol*. 1919;3:147–174.
22. Hinman F. Renal counterbalance. *Cal West Med*. 1926;24:333–335.
23. Finn WF. Renal counterbalance. *J Lab Clin Med*. 1985;105:523–530.
24. Le Clef N, Verhulst A, D'Haese PC, et al. Unilateral renal ischemia-reperfusion as a robust model for acute to chronic kidney injury in mice. *PLoS One*. 2016;11:e0152153.
25. Tod P, Bukosza EN, Róka B, et al. Post-ischemic renal fibrosis progression is halted by delayed contralateral nephrectomy: the involvement of macrophage activation. *Int J Mol Sci*. 2020;21:3825.
26. Róka B, Tod P, Kaucsár T, et al. Delayed contralateral nephrectomy halted post-ischemic renal fibrosis progression and inhibited the ischemia-induced fibromir upregulation in mice. *Biomedicines*. 2021;9:815.
27. Le Clef N. *Unilateral Ischemia-Reperfusion as a Model for Acute-to-Chronic Kidney Disease: Development and Application*. University of Antwerp; 2016.
28. Kierulf-Lassen C, Nielsen PM, Qi H, et al. Unilateral nephrectomy diminishes ischemic acute kidney injury through enhanced perfusion and reduced pro-inflammatory and pro-fibrotic responses. *PLoS One*. 2017;12:e0190009.
29. Xu L, Guo J, Moledina DG, et al. Immune-mediated tubule atrophy promotes acute kidney injury to chronic kidney disease transition. *Nat Commun*. 2022;13:4892.
30. Bouteldja N, Klinkhammer BM, Bülow RD, et al. Deep learning-based segmentation and quantification in experimental kidney histopathology. *J Am Soc Nephrol*. 2021;32:52–68.
31. Hänzelmann S, Castelo R, Guinney J. GSVA: gene set variation analysis for microarray and RNA-seq data. *BMC Bioinformatics*. 2013;14:7.
32. Fu J, Sun Z, Wang X, et al. The single-cell landscape of kidney immune cells reveals transcriptional heterogeneity in early diabetic kidney disease. *Kidney Int*. 2022;102:1291.
33. Shen WK, Zhang CY, Gu YM, et al. An automatic annotation tool and reference database for T cell subtypes and states at single-cell resolution. *Sci Bull (Beijing)*. 2025;70:1659–1672.
34. Yang JM, Zhang N, Luo T, et al. TCellSI: a novel method for T cell state assessment and its applications in immune environment prediction. *iMeta*. 2024;3:e231.

35. Papes F, Kemper EL, Cord-Neto G, et al. Lysine degradation through the saccharopine pathway in mammals: involvement of both bifunctional and monofunctional lysine-degrading enzymes in mouse. *Biochemical J*. 1999;344(pt 2):555.
36. Liu W, Le A, Hancock C, et al. Reprogramming of proline and glutamine metabolism contributes to the proliferative and metabolic responses regulated by oncogenic transcription factor c-MYC. *Proc Natl Acad Sci U S A*. 2012;109:8983–8988.
37. Javed K, Bröer S. Mice lacking the intestinal and renal neutral amino acid transporter SLC6A19 demonstrate the relationship between dietary protein intake and amino acid malabsorption. *Nutrients*. 2019;11:2024.
38. Horiba N, Masuda S, Takeuchi A, et al. Cloning and characterization of a novel Na+-dependent glucose transporter (NaGLT1) in rat kidney. *J Biol Chem*. 2003;278:14669–14676.
39. Obeidat M, Li L, Ballermann BJ. TIMAP promotes angiogenesis by suppressing PTEN-mediated Akt inhibition in human glomerular endothelial cells. *Am J Physiol Renal Physiol*. 2014;307:F623–F633.
40. Yang D, Yang H, Luiselli G, et al. Increased plasmin-mediated proteolysis of L1CAM in a mouse model of idiopathic normal pressure hydrocephalus. *Proc Natl Acad Sci U S A*. 2021;118:e2010528118.
41. Lim HY, Lim SY, Tan CK, et al. Hyaluronan receptor LYVE-1-expressing macrophages maintain arterial tone through hyaluronan-mediated regulation of smooth muscle cell collagen. *Immunity*. 2018;49:326–341.e7.
42. Dufour JH, Dziejman M, Liu MT, et al. IFN-gamma-inducible protein 10 (IP-10; CXCL10)-deficient mice reveal a role for IP-10 in effector T cell generation and trafficking. *J Immunol*. 2002;168:3195–3204.
43. Szabo SJ, Kim ST, Costa GL, et al. A novel transcription factor, T-bet, directs Th1 lineage commitment. *Cell*. 2000;100:655–669.
44. Sasaki I, Hoshino K, Sugiyama T, et al. Spi-B is critical for plasmacytoid dendritic cell function and development. *Blood*. 2012;120:4733–4743.
45. Ng SS, De Labastida Rivera F, Yan J, et al. The NK cell granule protein NKG7 regulates cytotoxic granule exocytosis and inflammation. *Nat Immunol*. 2020;21:1205–1218.
46. Papadimitriou TI, Singh P, van Caam A, et al. CD7 activation regulates cytotoxicity-driven pathology in systemic sclerosis, yielding a target for selective cell depletion. *Ann Rheum Dis*. 2023;83:488–498.
47. Denda-Nagai K, Aida S, Saba K, et al. Distribution and function of macrophage galactose-type C-type lectin 2 (MGL2/CD301b): efficient uptake and presentation of glycosylated antigens by dendritic cells. *J Biol Chem*. 2010;285:19193–19204.
48. Bachem A, Güttler S, Hartung E, et al. Superior antigen cross-presentation and XCR1 expression define human CD11c+CD141+ cells as homologues of mouse CD8+ dendritic cells. *J Exp Med*. 2010;207:1273–1281.
49. Sahara H, Shastri N. Second class minors: molecular identification of the autosomal H46 histocompatibility locus as a peptide presented by major histocompatibility complex class II molecules. *J Exp Med*. 2003;197:375.
50. Li Y, Ma H, Zhang Y, et al. PGLYRP2 drives hepatocyte-intrinsic innate immunity by trapping and clearing hepatitis B virus. *J Clin Invest*. 2025;135:e188083.
51. Westwell-Roper C, Denroche HC, Ehses JA, et al. Differential activation of innate immune pathways by distinct islet amyloid polypeptide (IAPP) aggregates. *J Biol Chem*. 2016;291:8908–8917.
52. Jablonski P, Howden B, Rae D, et al. The influence of the contralateral kidney upon recovery from unilateral warm renal ischemia. *Pathology*. 1985;17:623–627.
53. Skrypnyk NI, Harris RC, de Caestecker MP. Ischemia-reperfusion model of acute kidney injury and post injury fibrosis in mice. *J Vis Exp*. 2013;(78):50495.
54. Zhang J, Shen R, Lin H, et al. Effects of contralateral nephrectomy timing and ischemic conditions on kidney fibrosis after unilateral kidney ischemia-reperfusion injury. *Ren Fail*. 2022;44:1568–1584.
55. Bonvalet JP, Champion M, Wanstok F, et al. Compensatory renal hypertrophy in young rats: increase in the number of nephrons. *Kidney Int*. 1972;1:391–396.
56. Johnson HA, Vera Roman JM. Compensatory renal enlargement: hypertrophy versus hyperplasia. *Am J Pathol*. 1966;49:1–13.
57. Sammut S, Behr L, Hekmati M, et al. Compensatory renal growth after unilateral or subtotal nephrectomy in the ovine fetus. *Pediatr Res*. 2013;74:624–632.
58. Tsau YK, Tsai IJ, Chen YM. Transient reciprocal change of renal hepatocyte growth factor and transforming growth factor-beta1 may relate to renal hypertrophy in rats with liver injury or unilateral nephrectomy. *Pediatr Res*. 2006;59(pt 1):494–499.
59. Arfian N, Muflikhah K, Soeyono SK, et al. Vitamin D attenuates kidney fibrosis via reducing fibroblast expansion, inflammation, and epithelial cell apoptosis. *Kobe J Med Sci*. 2016;62:E38.
60. Kandula P, Dobre M, Schold JD, et al. Vitamin D supplementation in chronic kidney disease: a systematic review and meta-analysis of observational studies and randomized controlled trials. *Clin J Am Soc Nephrol*. 2011;6:50–62.
61. Tan X, Li Y, Liu Y. Therapeutic role and potential mechanisms of active Vitamin D in renal interstitial fibrosis. *J Steroid Biochem Mol Biol*. 2007;103:491–496.
62. Zhang Y, Kong J, Deb DK, et al. Vitamin D receptor attenuates renal fibrosis by suppressing the renin-angiotensin system. *J Am Soc Nephrol*. 2010;21:966–973.
63. Cantorna MT, Waddell A. The vitamin D receptor turns off chronically activated T cells. *Ann N Y Acad Sci*. 2014;1317:70–75.
64. Chang SH, Chung Y, Dong C. Vitamin D suppresses Th17 cytokine production by inducing C/EBP homologous protein (CHOP) expression. *J Biol Chem*. 2010;285:38751–38755.
65. Guillot X, Semerano L, Saidenberg-Kermanac'h N, et al. Vitamin D and inflammation. *Joint Bone Spine*. 2010;77:552–557.
66. Tang J, Zhou R, Luger D, et al. Calcitriol suppresses antiretinal autoimmunity through inhibitory effects on the Th17 effector response. *J Immunol*. 2009;182:4624–4632.